J Therm Anal Calorim (2012) 107:617–624
DOI 10.1007/s10973-011-1400-5

Thermal stability and crystallization kinetics of Pb and Bi borate-based glasses

Essam R. Shaaban · S. H. Mohamed

Received: 17 January 2011 / Accepted: 10 February 2011 / Published online: 25 February 2011

Abstract Glasses with compositions $60B_2O_3$–$40PbO$, $60B_2O_3$–$40Bi_2O_3$, and $60B_2O_3$–$30Bi_2O_3$–$10PbO$ have been prepared and studied by differential thermal analysis. The crystallization kinetics of the glasses was investigated under non-isothermal conditions. From dependence of the glass transition temperature (T_g) on the heating rate, the activation energy for the glass transition was derived. Similarly the activation energy of the crystallization process was determined. Thermal stability of these glasses were achieved in terms of the characteristic temperatures, such as the glass transition temperature, T_g, the onset temperature of crystallization, T_{in}, the temperature corresponding to the maximum crystallization rate, T_p, beside the kinetic parameters, $K(T_g)$ and $K(T_p)$. The results revealed that the $60B_2O_3$–$40PbO$ is more stable than the others. The crystallization mechanism is characterized for glasses. The phases at which the glass crystallizes after the thermal process have been identified by X-ray diffraction.

Keywords Borate-based glasses · Thermal stability · Crystallization kinetics · XRD analysis

Present Address:
E. R. Shaaban · S. H. Mohamed (✉)
Physics Department, College of Science, Qassim University,
P.O. Box 6644, Buryadh 51452, Kingdom of Saudi Arabia
e-mail: abo_95@yahoo.com

E. R. Shaaban
Department of Physics, Faculty of Science,
Al-Azahar University, Assiut 71542, Egypt

S. H. Mohamed
Physics Department, Faculty of Science,
Sohag University, Sohag 82524, Egypt

Introduction

Over the last decade, borate-based glasses have been studied from both academic and technological point of view. B_2O_3 is one of the most important glass formers incorporated into various kinds of glass systems as a flux material in order to obtain materials having specific physical and chemical properties suitable for technological applications. The boron atom in borate glasses and crystals usually coordinates with either three or four oxygen atoms forming $[BO_3]$ or $[BO_4]$ structural units. These two fundamental units can be arbitrarily combined to form either the so-called super-structure or different B_xO_y structural groups like boroxol ring, pentaborate, tetraborate, diborate groups, etc. The number of the structural units depends on the nature and the total concentration of the added modifiers [1–5]. In view of this, borate glasses containing Bi_2O_3 have attracted a considerable attention because of its wide applications in the field of glass–ceramics, thermal and mechanical sensors, reflecting windows, soil environment, and may be used as layers for optical and opto-electronic devices, etc. [6–10]. These glasses have a long infrared cut-off, and high third-order non-linear optical susceptibility which makes them ideal candidates for applications in the infrared transmission components, ultrafast optical switches, and photonic devices [11, 12]. Lead borate glasses are also of significant scientific and practical interest. Lead borate glasses are of technological interests owing to their unique properties such as wide glass formation regions and good radiation shielding properties [13–16]. During the past two decades, many efforts have been made to realize the roles of PbO in glass networks using different techniques. Honma et al. [17, 18] discovered the formation of new non-linear optical crystalline phases $Ln_xBi_{1-x}BO_3$ in the crystallized glasses of

Ln_2O_3–Bi_2O_3–B_2O_3 (Ln = La, Gd, Sm) and found that the crystallized glasses of Gd_2O_3–Bi_2O_3–B_2O_3 show strong second harmonic intensities compared with the crystallized glasses consisting of La_2O_3 or Sm_2O_3. Furthermore, they found that some glasses such as $12.5Sm_2O_3$–$30Bi_2O_3$–$57.5B_2O_3$ are crystallized by irradiations of a continuous Nd:YAG laser with a wavelength of $\lambda = 1064$ nm, giving the formation of non-linear optical crystalline dots and lines [17, 18].

The purpose of this study is to study and compare the thermal stability and crystallization kinetics of $60B_2O_3$–40PbO, $60B_2O_3$–$40Bi_2O_3$, and $60B_2O_3$–$30Bi_2O_3$–10PbO glasses. Thermal stability of these glasses were achieved in terms of the characteristic temperatures such as the glass transition temperature, T_g, the onset temperature of crystallization, T_{in}, the temperature corresponding to the maximum crystallization rate, T_p, of differential thermal analysis (DTA) curves of different heating rates beside the kinetic parameters as a function of glass transition temperature $K(T_g)$ and the maximum crystallization temperature $K(T_p)$. The phases at which the glasses crystallize after the thermal process have been identified by X-ray diffraction.

Experimental procedures

The glass samples of the general chemical formula $60B_2O_3$–40PbO, $60B_2O_3$–$40Bi_2O_3$, $60B_2O_3$–$30Bi_2O_3$–10PbO, and $60B_2O_3$–$30Bi_2O_3$–$10Gd_2O_3$ glasses have been prepared by the melt quenching technique. Required quantities of Analar grade H_3BO_3, Bi_2O_3, and PbO were mixed together by grinding the mixture repeatedly to obtain a fine powder. The mixture was melted in a Porcelain crucible in an electrically heated furnace under ordinary atmospheric conditions at temperature about 1273 K for 2 h to homogenize the melt. The glass samples, obtained from the quickly melt quenching, were put into preheated stainless-steel mold and heat-treated at a temperature of about 20 K below their calorimetric glass transition temperature for 2 h to remove any internal stresses. The composition refers to the nominal composition (the starting mixture). To check the non-crystallinity of the glass samples, X-ray diffraction measurements were performed using a Philips X-ray diffractometer PW/1710 with Ni-filtered, Cu-K_α radiation ($\lambda = 1.542$ Å) powered at 40 kV and 30 mA. The results showed that XRD patterns of the glasses did not reveal discrete or any sharp peaks, but the characteristic broad humps of the amorphous materials.

The calorimetric measurements were carried out using a differential thermal analysis calorimeter type Shimadzu 50 with an accuracy of ±0.1 K. The calorimeter was calibrated, for each heating rate, using well-known melting temperatures and the melting enthalpies of zinc and indium supplied with the instrument. The glass powders weighing 20 mg were contained in an alumina crucible and the reference material was α-alumina powder. The samples were heated in air at heating rates β of 5, 10, 20, 30, and 40 K min^{-1}. The value of the glass transition, T_g, the extrapolated crystallization onset, T_{in}, and the crystallization peak temperature, T_p, and melting temperature were determined with an accuracy of ±1 K by using the microprocessor of the thermal analyzer.

The criterion parameters of the thermal stability

The criterion parameters are based on characteristic temperatures such as the glass transition temperature, T_g, the onset temperature of crystallization $T_{in,}$ the temperature corresponding to maximum crystallization rate, T_p and the melting temperature, T_m. Dietzel [19] introduced the glass criterion, $\Delta T = T_{in} - T_g$, which is often an important parameter to evaluate the glass forming ability. The thermal stability of glasses according to Sakka and Mackenzie [20] was achieved by using the ratio T_g/T_m. By the use of the characteristic temperatures, Hruby [21] developed the H_r criterion, $H_r = \Delta T/(T_m - T_p)$. Saad and Poulain [22] obtained another two criteria, weighted the thermal stability $H'(H' = \Delta T/T_g)$ and the S criterion $(S = (T_p - T_{in})\ \Delta T/T_g)$. The glass-forming ability can be calculated by using the relation, $k_{gl} = (T_{in} - T_g)/(T_m - T_g)$. The higher values of the criterion parameters reflect the greater thermal stability of the glass.

On the other hand, the formal theory of transformation kinetics describes the evolution of the volume fraction crystallized, χ, in terms of the crystal growth, u with time t:

$$\chi = 1 - \exp\left[-g\left(\int_0^t u\mathrm{d}t'\right)^n\right] = 1 - \exp(-I_1^n) \qquad (1)$$

where g is a geometric factor and n is an exponent, which depends on the mechanism of transformation. Derivation of Eq. 1 with respect to time and taking into account the Arrhenian temperature dependence for the crystal growth rate [18], the crystallization rate is obtained as

$$\frac{\mathrm{d}\chi}{\mathrm{d}t} = n(1-\chi)I_1^{n-1}K_0\exp\left(\frac{-E}{RT}\right) = nK(1-\chi)I_1^{n-1} \qquad (2)$$

where E is the effective activation energy for crystal growth and K is the reaction rate constant which has an Arrhenian temperature dependence according to the relation

$$K(T) = K_0 \exp(-E/RT) \quad (3)$$

Surinach et al. [23] and Hu et al. [24] introduced two criterion,

$$K(T_g) = K_0 \exp(-E/RT_g) \quad (4a)$$

and

$$K(T_p) = K_0 \exp(-E/RT_p) \quad (4b)$$

The values of last two parameters indicate the tendency for glass devitrification on heating; whereas the glass formation is a kinetic process.

Results and discussion

Thermal stability of glasses

Figure 1 shows the DTA thermograms of amorphous $60B_2O_3$–$40PbO$, $60B_2O_3$–$40Bi_2O_3$, and $60B_2O_3$–$30Bi_2O_3$–$10PbO$ glasses recorded at heating rate $\beta = 10$ K min^{-1}. The characteristic feature of this thermogram is the homogeneity of the considered glasses which is confirmed by the appearance of a small single endothermic peak. This peak is attributed to the glass transition temperature, which represents the strength or rigidity of the glass structure. Also, there is an exothermic peak originating from the amorphous-crystalline transformation. The exothermic peak has two characteristic points: the first point is the onset temperature of crystallization (T_{in}) and the second is the peak temperature of crystallization (T_p). This figure also shows a sharp endothermic peak which is the characteristic of the melting temperatures (T_m).

The characteristic temperatures T_g, T_{in}, T_p, and T_m for $60B_2O_3$–$40PbO$, $60B_2O_3$–$40Bi_2O_3$, and $60B_2O_3$–$30Bi_2O_3$–$10PbO$ glasses are given in Table 1. The glass forming ability of the studied glasses can be estimated by using

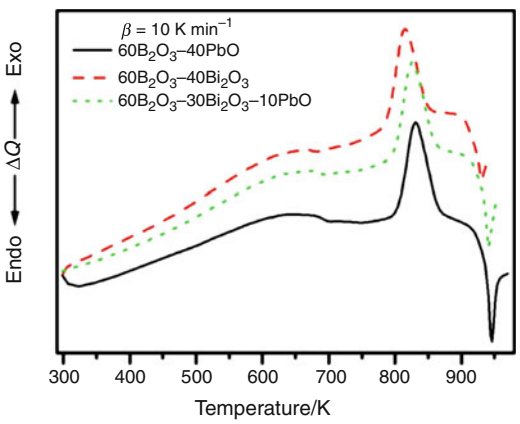

Fig. 1 Typical DTA trace of $60B_2O_3$–$40PbO$, $60B_2O_3$–$40Bi_2O_3$, and $60B_2O_3$–$30Bi_2O_3$–$10PbO$ glasses

Table 1 The values of thermal parameters of glass transition temperature T_g, onset temperature of crystallization T_{in}, crystallization temperature T_p, and melting temperature T_m of $60B_2O_3$–$40PbO$, $60B_2O_3$–$40Bi_2O_3$, and $60B_2O_3$–$30Bi_2O_3$–$10PbO$ glasses with different heating rates β. The characteristic parameters K_{gl}, H_r, and S according to the text

Alloy	β	T_g/K	T_{in}/K	T_p/K	T_m/K	K_{gl}	H_r	H'	S/K
$60B_2O_3$–$40PbO$	5	674	795	817	940	0.83	0.98	0.18	3.94
	10	684	806	827	950	0.84	0.98	0.18	3.74
	20	696	818	837	962	0.84	0.97	0.17	3.32
	30	702	823	843	972	0.81	0.93	0.17	3.44
	40	706	828	848	981	0.79	0.91	0.17	3.45
$60B_2O_3$–$40Bi_2O_3$	5	667	779	801	926	0.76	0.90	0.17	3.74
	10	679	790	811	936	0.76	0.89	0.16	3.48
	20	692	802	821	948	0.75	0.87	0.16	3.06
	30	697	807	827	958	0.73	0.84	0.16	3.20
	40	702	812	832	967	0.71	0.82	0.16	3.17
$60B_2O_3$–$30Bi_2O_3$–$10PbO$	5	671	787	809	931	0.81	0.96	0.17	3.82
	10	682	798	819	941	0.82	0.96	0.17	3.58
	20	695	810	829	953	0.81	0.93	0.17	3.15
	30	700	815	835	963	0.78	0.90	0.16	3.30
	40	705	820	840	972	0.76	0.88	0.16	3.27

these characteristic temperatures. The existing stability criterion parameters based on these characteristic temperatures H_r, H' and S for both compositions is listed in Table 1. It is found that, the values of these criteria are highest for $60B_2O_3$–$40PbO$ and lowest for $60B_2O_3$–$40Bi_2O_3$, indicating that $60B_2O_3$–$40PbO$ is more thermally stable**.** It was previously reported that the higher Bi_2O_3 content of the alloy, the lower its glass stability [25–27].

The activation energy of the glass transition, E_g, for investigated glasses has been obtained by using the Kissinger formula, which was originally derived for the crystallization process but which is also valid for the glass transition [28]. The formula has the following form

$$\ln(T_g^2/\beta) = E_g/RT_g + const. \quad (5)$$

where R is the universal gas constant. By fitting the plot between $\ln(T_g^2/\beta)$ and $1/T_g$ to straight line the values of E_g (see Fig. 2) can be obtained, where the subscript g denotes the magnitude values corresponding to the glass transition temperature. The values of the activation energy obtained for the glasses are found to be 241.2 kJ mol^{-1} for $60B_2O_3$–$40PbO$, 219.1 for $60B_2O_3$–$40Bi_2O_3$, and 227 kJ mol^{-1} for $60B_2O_3$–$30Bi_2O_3$–$10PbO$.

For the evaluation of activation energy for crystallization (E_c) by using the variation of T_p with β, Vázquez et al. [28] developed the proposed method by Kissenger for non-isothermal analysis of devitrification as follows:

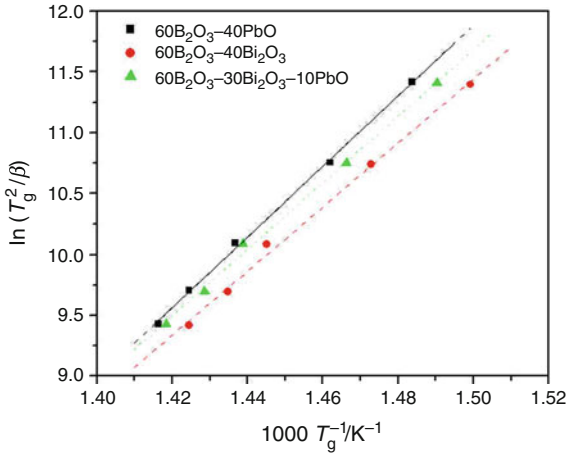

Fig. 2 Plots of $\ln(T_g^2/\beta)$ versus $1000/T_g$ and straight regression *lines* for the analyzed materials

$$\ln[T_p^2/\beta] = E_c/RT_p + \ln(E_c/RK_0) \quad (6)$$

This equation represents a straight line between $\ln(T_p^2/\beta)$ and $1/T_p$, for different compositions whose slopes yield a value of E_c (see Fig. 3). The values of the activation energy obtained for the glasses are found to be 375.7 kJ mol^{-1} for $60B_2O_3$–40PbO, 361.8 for $60B_2O_3$–$40Bi_2O_3$, and 368.7 kJ mol^{-1} for $60B_2O_3$–$30Bi_2O_3$–10PbO. The intercept of Eq. 6 is ln (E_c/RK_0). Then, one can obtain E_c and K_0.

After knowing the values of E_c and K_0, the kinetic parameters $K(T_g)$ and $K(T_p)$ of studied glasses were calculated using Eq. 4a and 4b, respectively. These calculations were carried out in order to compare the stability sequence of the studied glasses from the quoted parameters with the corresponding sequence deduced from the stability criteria based on characteristic temperatures. The values

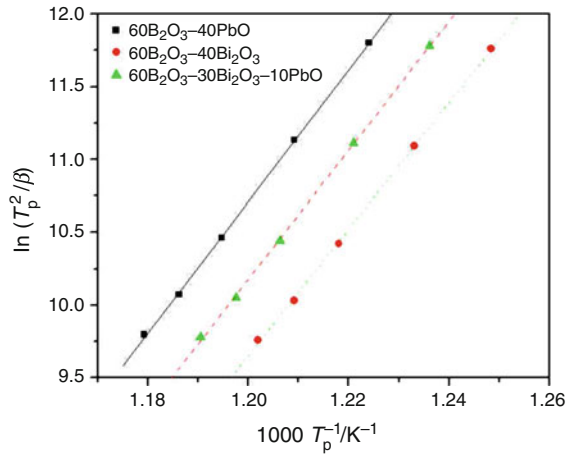

Fig. 3 Plots of $\ln(T_p^2/\beta)$ versus $1000/T_p$ and straight regression *lines* for the analyzed materials

of $K(T_g)$ and $K(T_p)$ of the temperatures T_g and T_p are calculated at different heating rates β as shown in Fig. 4a and b, respectively. According to the literature [29, 30], the smaller the values of $K(T_g)$ and $K(T_p)$ criteria, the better should be the glass forming ability of the material. So, the data for both $K(T_g)$ and $K(T_p)$ in Fig. 5a and b indicate that the thermal stability of $60B_2O_3$–40PbO glass is higher than other glasses.

Crystallization rate and kinetic exponent

The theoretical basis for interpreting DTA results is provided by the formal theory of transformation kinetics as developed by Johnson et al. [31] and Avrami [32, 33]. The fraction, χ, crystallized at a given temperature, T, is given by $\chi = A_T/A$ where A, is the total area of the exothermic between the temperature, T_i (crystallization is just beginning) and the temperature, T_f (the crystallization is completed), and A_T is the area between T_i and T, as shown in Fig. 6. The graphical representations of the crystallized

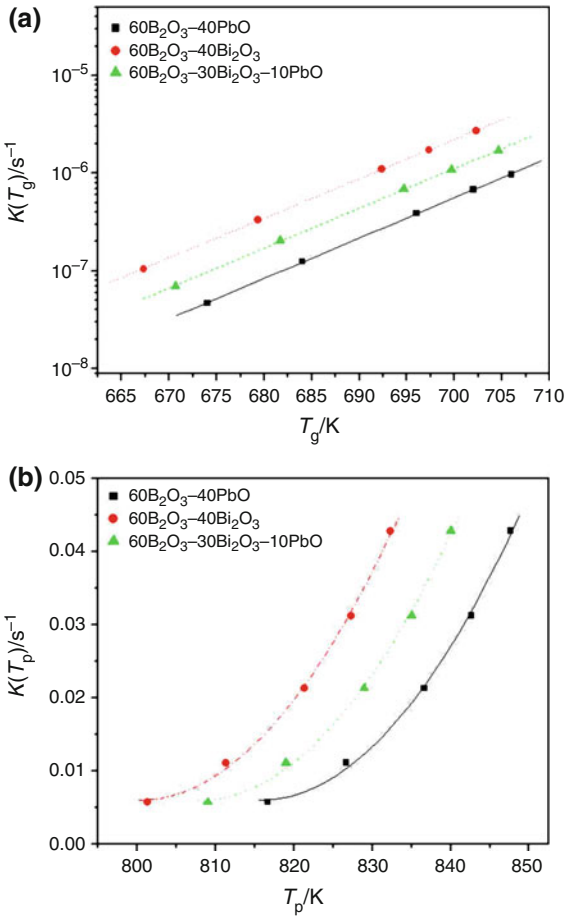

Fig. 4 **a** Plots of $K(T_g)$ versus T_g for the different glass compositions. **b** Plots of $K(T_p)$ versus T_p for the different glass compositions

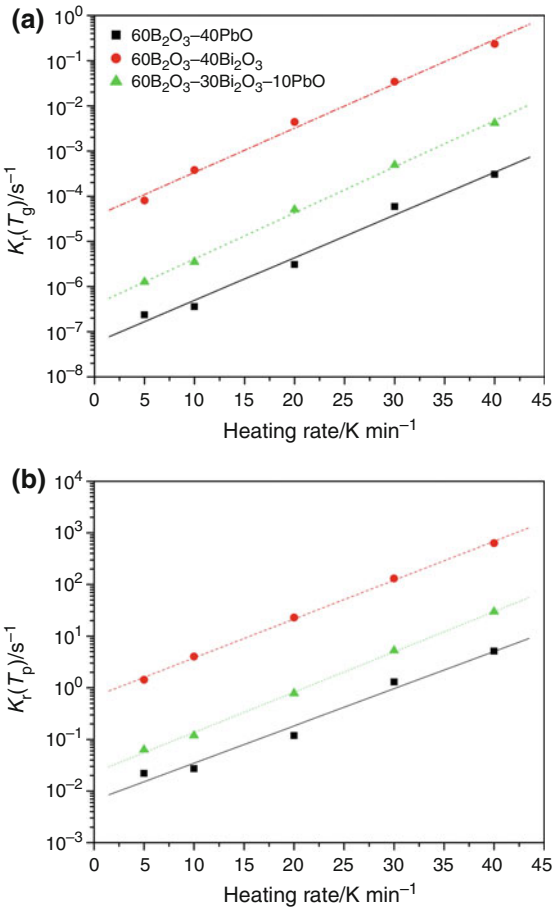

Fig. 5 **a** Plots of $K_r(T_g)$ versus β for the different glass compositions. **b** Plots of $K_r(T_g)$ versus β for the different glass compositions

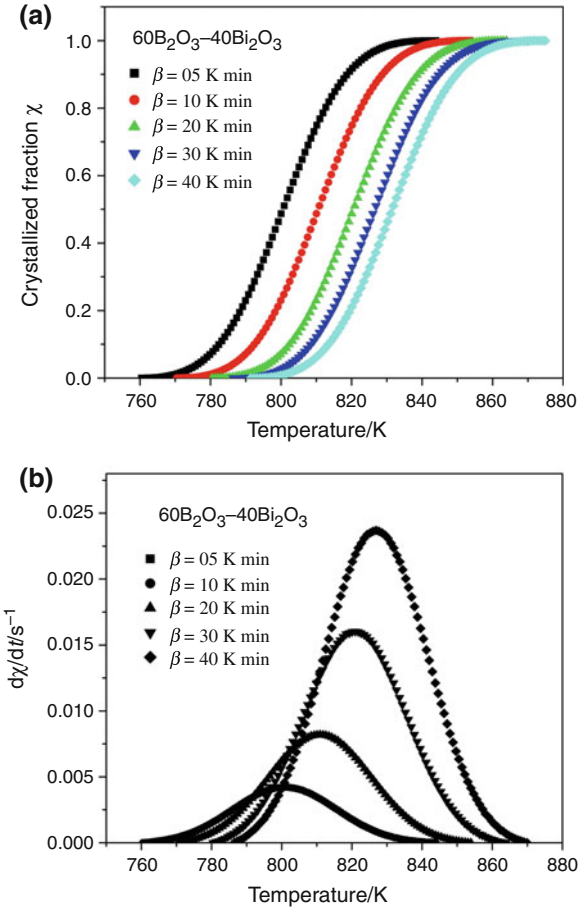

Fig. 7 **a** The crystallized fraction as a function of temperature for $60B_2O_3$–$40Bi_2O_3$ glass. **b** Crystallization rate versus temperature of the exothermal peaks for $60B_2O_3$–$40Bi_2O_3$ glass

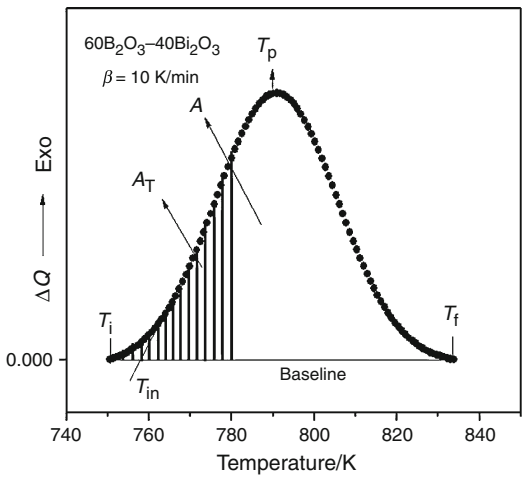

Fig. 6 DTA traces for $60B_2O_3$–$40Bi_2O_3$ glass at heating rate 10 K min^{-1}. The *vertical lines* show the area A_T between T_i and T of the peak. T_i, T_f, and T are according to the text

volume fraction of $60B_2O_3$–$40Bi_2O_3$ at different heating rates show the typical sigmoid curve as a function of temperature as shown in Fig. 7a [34, 35].

The ratio between the ordinates of the DTA curve and the total area of the peak gives the corresponding crystallization rates, which makes it possible to build the curves of the exothermal peaks represented in Fig. 7b for $60B_2O_3$–$40Bi_2O_3$ sample. The crystallization rate, $(d\chi/dt)_p$ values increases with increasing the heating rate, which has been widely discussed in the literature [27, 30].

From the experimental data, T_p, and $(d\chi/dt)_p$, listed in Tables 1 and 2, and the above mentioned values of the activation energies of crystallization process for the crystallization peaks, it makes possible to determine the kinetic exponent, n, at different heating rates using the following relation:

$$(d\chi/dt)_p = n(0.37\beta E_c)/(RT_p^2) \quad (7)$$

The values of n are listed in Table 2. The average kinetic exponent for different glasses is listed in Table 2. Taking into account the experimental error, the value of $\langle n \rangle$ is close to 2 for the two binary systems of $60B_2O_3$–40PbO and $60B_2O_3$–$40Bi_2O_3$ glass and close to 3 for the ternary system of $60B_2O_3$–$30Bi_2O_3$–10PbO. The kinetic exponent

Table 2 Maximum crystallization rate $(d\chi/dt)$, kinetic exponent n and average kinetic exponent $\langle n \rangle$ for different composition with different heating rates β

Composition	$60B_2O_3$–40PbO		$60B_2O_3$–$40Bi_2O_3$		$60B_2O_3$–$30Bi_2O_3$–10PbO	
β/K min^{-1}	$(d\chi/dt) \times 10^{-3}/s^{-1}$	n	$(d\chi/dt) \times 10^{-3}/s^{-1}$	n	$(d\chi/dt) \times 10^{-3}/s^{-1}$	n
5	4.62	2.2	4.21	2.01	5.46	2.61
10	9.01	2.2	8.21	2.01	10.7	2.61
20	17.6	2.2	16	2.01	20.8	2.61
30	26	2.2	23.7	2.01	30.8	2.61
40	34.3	2.21	31.2	2.01	40.5	2.61
$\langle n \rangle$		**2.212**		2.012		**2.614**

was deduced based on the mechanism of crystallization [36]. According to Mahadevan et al. [37] n may be 4, 3, 2 or 1 which are related to the different glass-crystal transformation mechanisms: $n = 4$, volume nucleation, three-dimensional growth; $n = 3$, volume nucleation, two-dimensional growth, $n = 2$, volume nucleation, one-dimensional growth; $n = 1$, surface nucleation, one-dimensional growth from surface to the inside. Therefore, $\langle n \rangle = 2$ and $\langle n \rangle = 3$, crystallization mechanism proceeds by one and two-dimensional growth, respectively, with volume nucleation in both cases.

Identification of the crystalline phases

The identification of the possible phases, which crystallize during the thermal treatment, has been carried out by means of XRD measurements. The X-ray diffraction patterns of $60B_2O_3$–40PbO glass annealed at 825 K for 2 h, $60B_2O_3$–$40Bi_2O_3$ glasses annealed at 810 K and also $60B_2O_3$–$30Bi_2O_3$–10PbO annealed at 815 K as shown in Fig. 8. The diffractogram of the transformed material of $60B_2O_3$–40PbO after the crystallization process suggests the presence of microcrystallites of a single phase of lead borate, PbB4O7 according to JCPDS (card no. 15-0278), which crystallizes to the orthorhombic crystal system, with lattice parameters $a = 4.243$ nm, $b = 10.840$ nm, and $c = 4.243$ nm. The diffractogram of the transformed material of $60B_2O_3$–$40Bi_2O_3$ after the crystallization process suggests the presence of microcrystallites of a single phase. From the JCPDS files these peaks can be identified as bismuth borate, BiBO3, (card no. 27-0320), which crystallizes to unknown crystal system. The diffractogram of the transformed material for $60B_2O_3$–$30Bi_2O_3$–10PbO, after the crystallization process, suggests the presence of microcrystallites of two phases. From the JCPDS files these peaks can be identified as $BiBO_3$ (card no. 27-0320) and orthorhombic $Bi_3B_5O_{12}$ (card no. 28-0228) with lattice parameters $a = 6.532$ nm, $b = 7.733$ nm, and $c = 18.566$ nm. No phases were detected for lead borate.

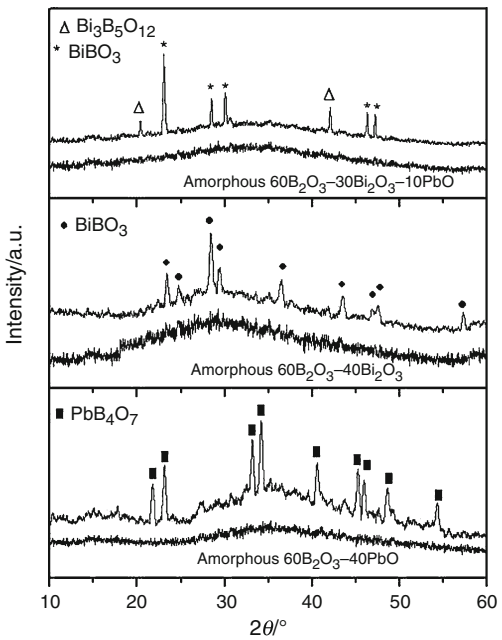

Fig. 8 XRD patterns of amorphous and crystallized $60B_2O_3$–40PbO, $60B_2O_3$–$40Bi_2O_3$, and $60B_2O_3$–$30Bi_2O_3$–10PbO glasses

Conclusions

The non-isothermal devitrification of $60B_2O_3$–40PbO, $60B_2O_3$–$40Bi_2O_3$, and $60B_2O_3$–$30Bi_2O_3$–10PbO glasses have been studied at different heating rates. The glass forming ability of $60B_2O_3$–40PbO, $60B_2O_3$–$40Bi_2O_3$ and $60B_2O_3$–$30Bi_2O_3$–10PbO glasses have been evaluated by using various thermal stability criteria, based on characteristic temperatures beside the kinetic parameters, $K(T_g)$ and $K(T_p)$. It is reasonable to think that the obtained data from the quoted criteria agree satisfactorily with the values which result from the existing criteria based on characteristic temperatures and kinetic parameters $K(T_g)$ and $K(T_p)$ criteria. A lower value of $K(T_g)$ and $K(T_p)$ means higher stability of the glass. Glass composition of $60B_2O_3$–40PbO is more stable than the other glasses. The crystallization

mechanism was characterized for studied glasses. The binary $60B_2O_3$–$40PbO$ and $60B_2O_3$–$40Bi_2O_3$ glasses have kinetic exponent $n = 2.212$ and $n = 2.012$, respectively. The crystallization mechanism for ternary glass 40PbO, $60B_2O_3$–$30Bi_2O_3$–10PbO has kinetic exponent $n = 2.614$.

The identification of the crystalline phases was made by recording the X-ray diffraction pattern of the transformed material. This pattern shows the existence of microcrystallites of single phase of PbB_4O_7 in amorphous matrix for annealed $60B_2O_3$–$40PbO$ glass and single phase of $BiBO_3$ in amorphous matrix for the annealed $60B_2O_3$–$40Bi_2O_3$ glass. However, the diffractogram of $60B_2O_3$–$30Bi_2O_3$–10PbO, after the crystallization process, suggests the presence of microcrystallites of $BiBO_3$ and $Bi_3B_5O_{12}$ phases and no indication for lead borate phases.

Acknowledgements The authors thank Sabic Company through the Deanship of Scientific Research at Qassim University for financial support under contract no. SR-S-009-07.

References

1. Fukawa Y, Matsuda Y, Kawashima M, Kojima S. Determination of complex-specific heat and fragility of sodium borate glasses by temperature-modulated DSC. J Therm Anal Calorim. 2010;99:39–44.
2. Venkataraman B, Varma K. Structural and optical properties of $(100 - x)(Li_2B_4O_7) - x(SrO–Bi_2O_3–0.7Nb_2O_5–0.3V_2O_5)$ glasses and glass nanocrystal composites. Opt Mater. 2006;28:1423–9.
3. Dutta A, Ghosh A. Structural and optical properties of lithium barium bismuthate glasses. J Non-Cryst Solids. 2007;353:1333–4.
4. Stone CE, Wright AC, Sinclair RN, Feller SA, Affatigato M, Hogan DL, Nelson ND, Vira C, Dimitriev YB, Gattef EM, Ehrt D. Structure of bismuth borate glasses. Phys Chem Glasses. 2000;41:409–12.
5. Wang S, Tan Z, Li Y, Sun L, Zhang T. Synthesis, characterization and thermal analysis of polyaniline/ZrO_2 composites. Thermochim Acta. 2006;441:191–4.
6. Zheng H, Mackenzie J. $Bi_4Sr_3Ca_3$ Cu_4O_{16} glass and superconducting glass ceramics. Phys Rev B. 1988;38:7166–8.
7. Hu Y, Lin U-L, Liu N-H. Effect of copper valence on the glass structure and crystallization behavior of Bi–Pb–Cu–O glasses. Mater Chem Phys. 1997;49:115–9.
8. Szumera M, Wacławska I, Olejniczak Z. Influence of B_2O_3 on the structure and crystallization of soil active glasses. J Therm Anal Calorim. 2010;99:879–86.
9. Onishi M, Kyoto M, Watanabe M. Properties of Bi–Pb–Sr–Ca–Cu–O glass-ceramic fibers formed by glass-drawing method. Jpn J Appl Phys. 1991;30:L988–90.
10. Yinnon H, Uhlmann DR. Applications of thermoanalytical techniques to the study of crystallization kinetics in glass-forming liquids, part I: theory. J Non-Cryst Solids. 1983;54:253–75.
11. Simon S, Todea M. Spectroscopic study on iron doped silica-bismuthate glasses and glass ceramics. J Non-Cryst Solids. 2006;352:2947–51.
12. Pan Z, Morgan SH, Long BH. Raman scattering cross-section and non-linear optical response of lead borate glasses. J Non-Cryst Solids. 1995;185:127–8.
13. Wu JM, Huang HL. Microwave properties of zinc, barium and lead borosilicate glasses. J Non-Cryst Solids. 1999;260:116–9.
14. Srivastava P, Rai SB, Rai DK. Effect of lead oxide on optical properties of Pr^{3+} doped some borate based glasses. J Alloys Compd. 2004;368:1–8.
15. Lower NP, McRae JL, Feller HA, Betzen AR, Kapoor S, Affatigato M, Feller SA. Physical properties of alkaline-earth and alkali borate glasses prepared over an extended range of compositions. J Non-Cryst Solids. 2001;293:669–75.
16. Liu HS, Chin TS, Yung SW. FTIR and XPS studies of low-melting PbO–ZnO–P_2O_2 glasses. Mater Chem Phys. 1997;50:1–11.
17. Honma T, Benino Y, Fujiwara T, Sato R, Komatsu T. New optical nonlinear crystallized glasses and YAG laser-induced crystalline dot formation in rare-earth bismuth borate system. Opt Mater. 2002;20:27–33.
18. Honma T, Benino Y, Fujiwara T, Komatsu T, Sato R. Nonlinear optical crystal-line writing in glass by yttrium aluminium garnet laser irradiation. Appl Phys Lett. 2003;82:892–3.
19. Dietzel A. Glass structure and glass properties. Glasstech. 1968;22:41.
20. Sakka S, Mackenzie JD. Relation between apparent glass transition temperature and liquids temperature for inorganic glasses. J Non-Cryst Solids. 1971;6:145–62.
21. Hruby A. Evaluation of glass-forming tendency by means of DTA. Czech J Phys B. 1972;22:1187–93.
22. Saad M, Poulain M. Glass forming ability criterion. Mater Sci Forum. 1987;19:11.
23. Surinach S, Baro MD, Clavaguera-Mora MT, Clavaguera N. Glass formation and crystallization in the $GeSe_2$–Sb_2Te_3 system. J Mater Sci. 1984;19:3005–12.
24. Hu L, Jiang Z, Chin J. A new criterion for crystallization of glass. Ceram Soc. 1990;18:315–21.
25. Shaaban ER, Shapaan M, Saddeek YB. Structural and thermal stability criteria of Bi_2O_3–B_2O_3 glasses. J Phys: Condens Matter. 2008;20:155108–9.
26. Baia L, Stefan R, Kiefer W, Popp J, Simon S. Structural investigations of copper doped B_2O_3–Bi_2O_3 glasses with high bismuth oxide content. J Non-Cryst Solids. 2002;303:379–86.
27. Lide D. CRC handbook of chemistry and physics. 84th ed. Boca Raton: CRC Press; 2004.
28. Vazquez J, Lopez-Alemany PL, Villares P, Jimenez-Garay R. Generalization of the Avrami equation for the analysis of non-isothermal transformation kinetics. Application to the crystallization of the $Cu_{0.20}As_{0.30}Se_{0.50}$ alloy. J Phys Chem Solids. 2000;61:493–500.
29. Mehta N, Agarwal P, Kumar A. Calorimetric studies of glass forming ability and thermal stability in a-Se 80Te 19.5 M 0.5(M = Ag, Cd, In, Sb) alloys. Eur Phys J Appl Phys. 2005;31:153–6.
30. Shaaban ER, Dessouky MT, Abousehly AM. Glass forming tendency in ternary $Ge_xAs_{20}Te_{80-x}$ glasses examined using differential scanning calorimetry. J Phys: Condens Matter. 2007;19:096212-11.
31. Johnson WA, Mehl RF. Reaction kinetics in processes of nucleation and growth. Trans Am Inst Min Met Eng. 1939;135:416–58.
32. Avrami M. Kinetics of phase change. II transformation-time relations for random distribution of nuclei. J Chem Phys. 1940;8:212–24.
33. Avrami M. Granulation, phase change, and microstructure kinetics of phase change. III. J Chem Phys. 1941;9:177–84.

34. Arora A, Shaaban ER, Singh K, Pandey OP. Non-isothermal crystallization kinetics of ZnO–BaO–B_2O_3–SiO_2 glass. J Non-Cryst Solids. 2008;354:3944–51.
35. Goel A, Shaaban ER, Tulyaganov DU, Ferreira JMF. Study of crystallization kinetics in glasses along the diopside–Ca-Tschermak join. J Am Ceram Soc. 2008;91:2690–8.
36. Matusita K, Saka S. Kinetic study of crystallization of glass by differential thermal analysis—criterion on application of Kissinger plot. J Non-Cryst Solids. 1980;38–39:741–6.
37. Mahadevan S, Giridhar A, Sing AK. Calorimetric measurements on As–Sb–Se glasses. J Non-Cryst Solids. 1986;88:11–34.